FIBRE-REINFORCED
CONCRETE

A case study on the spatial variability of strength in a SFRSCC slab and its correlation with fibre orientation

Dmitri Kartofelev[a], Oksana Goidyk[a], and Heiko Herrmann[a*]

[a] Department of Cybernetics, Tallinn University of Technology, Akadeemia tee 21, 12618 Tallinn, Estonia

Abstract. This paper presents the results of an experimental investigation into the effects of the fibre orientation and the concrete casting method on the flexural strength and fracture toughness of steel fibre reinforced self-compacting concrete (SFRSCC). A destructive four-point bending testing is used to measure the flexural strength at the main cracking, the accepted mean post-cracking loading, and the energy absorption capacity (toughness) of the concrete. It is shown that a *favourable* fibre orientation increases flexural strength up to 25%, the accepted mean post-cracking loading up to 65%, and the toughness up to 65% for the specific concrete mixture and concrete beams used. The presented results and analysis demonstrate the importance of the spatial fibre orientation and distribution on the final strength and durability of hardened concrete. The main findings and conclusions of this paper can also be extended to other fibre reinforced composite materials.

Key words: open pour concrete casting, material strength, free-surface flow, fibre orientation, four-point bending test, concrete reinforcement, concrete cracking, crack control, structural concrete elements.

1. INTRODUCTION

Concrete is one of the most widely used building materials that has developed considerably in the last 40 years, during which time its worldwide use has significantly increased [1]. It is first and foremost due to the use of fibre reinforced composites as construction materials that have improved many important aspects of modern buildings. Composites have decreased overall construction times and at the same time increased overall structural durability, impact, fire and corrosion resistance. They allow for higher strength at lower weight and lift various restrictions on previously non-feasible designs [2,3]. One such composite material is steel fibre reinforced self-compacting concrete (SFRSCC). It is often believed that in addition to time savings it also reduces the amount of skilled labour required on building sites, and as a result, is a source of financial savings [4,5].

Previous studies of SFRSCC have established that favourable mechanical properties of SFRSCC depend strongly on the average fibre orientation. Superior strength is achieved when fibres are oriented mostly in the dominant direction of tensile stresses present in a final product, which has been shown experimentally [6–12] and is in accordance with various theories [13–16]. The final orientation of the fibres within the hardened concrete is influenced by several factors: most importantly, the so-called "wall effects" of the

---

* Corresponding author, hh@cens.ioc.ee

casting formwork/molds [17,18]; pouring of the concrete and other nuances of the casting method used [19]; geometry and size of formwork [20,21]. Additionally, the amount and type of fibre have an impact on the post-cracking behaviour of SFRSCC. In particular, hooked-end fibres can show deflection-hardening behaviour, while straight fibres demonstrate the deflection-softening response [22]. Similarly, a low fibre amount leads to strain-softening while a higher fibre dosage is necessary to achieve strain-hardening. Different fibre materials, fibre geometry, and fibre amounts change the mechanical properties and post-cracking dynamics. For instance, the addition of medium or high strength steel fibres significantly increases the tensile and flexural strength of SFRSCC [23,24], whereas polyolefin fibres are chemically inert, able to control micro cracking occurring at the initial shrinkage stage of concrete hardening, and strengthen thus the interfacial bonds between the fibres and the concrete matrix [25]. Several research groups [26,27] have also considered hybrid fibre concretes that contain a mixture of different fibre types and materials, where each type of fibres has its own function and contribution to the cracking control. Some research has been done on the effect of the fibre content and fibre orientation on concrete fatigue under static and cyclic bending tests [28].

In order to predict or estimate the fibre orientation and dispersion, both during and after concrete casting, computational fluid dynamics modelling has been used. Kang and Kim [29] have analysed the dynamics of the flow-dependent fibre orientation, where for the sake of simplicity the interactions between fibres were neglected. They show that the fibres tend to align/orient in parallel with respect to the main flow direction in the case of shear flow, and perpendicular in the case of radial flow. This was shown to be especially true for increased distances from the casting point. Svec et al. [30] have presented a modified method that combines the lattice Boltzmann modelling with the corrected immersed boundary methods and a mass tracking algorithm allowing to simulate the SFRSCC flow as a non-Newtonian fluid. Herrmann and Lees [17] have performed the simulations of multiphase free-surface flow by using OpenFOAM 2.3.0 library [31]. They show that the influence of the surface properties of a casting formwork should be taken into account when modelling SFRSCC casting.

The aim of this case study is to present the quantitative results of an experimental investigation into the effects of the fibre orientation and the concrete casting method on the flexural strength and fracture toughness of SFRSCC. This paper is organized as follows. Section 2 describes in detail the experimental methodology applied. Section 3 presents the main findings: comparison of SFRSCC to standard self-compacting concrete (SCC) (Sec. 3.1); effects of the fibre orientation on flexural strength (Sec. 3.2); effects of the fibre orientation on the accepted mean post-cracking loading (Sec. 3.3); effects of the fibre orientation on post-cracking absorbed energy (Sec. 3.4); relationships between SFRSCC strength and crack positions (Sec. 3.5). Section 4 analyses the results of the experimental investigation and Section 5 presents a summary of the findings along with recommendations based on the analysed data.

2. EXPERIMENTAL METHODOLOGY

2.1. Main approach, theoretical and working assumptions

Two flat slabs with dimensions of 1.0 m $\times$ 0.1 m $\times$ 4.0 m are cast, using SCC and SFRSCC. After hardening, the SCC slab is cut by hand-held water-cooled diamond saw into 12 beams in the size of 0.1 m $\times$ 0.1 m $\times$ 1.0 m, approximately. The SFRSCC slab is cut into 40 beams in the size of $b \times h \times 1.0$ m, where the average beam cross-section width $b = 0.096$ m with the standard deviation of 0.0027 m and the average beam cross-section height $h = 0.105$ m with the standard deviation of 0.0014 m (normal and non-correlated distribution of beam cross-section dimensions is assumed). The layout and position of the cut-out beams with respect to the original slab is shown in Fig. 1.

The concrete casting process of the slabs used in this study is no different from the ordinary casting procedure implemented in civil engineering when creating similar structural concrete elements. The wet SFRSCC mixture is poured directly from a casting bucket into a formwork. The pouring and the consequent free-surface flow is initiated at the *casting point* (see Fig. 1) near one end of the slab. The casting point is
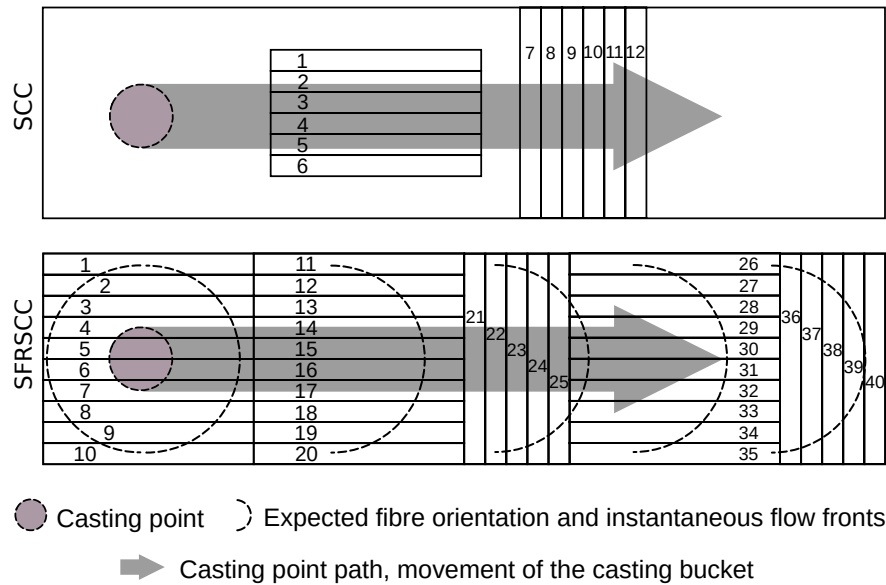
Fig. 1. Schematic drawing of the top view of the studied concrete slabs. Segmentation of the slab into smaller beams totalling 12 in the case of SCC and 40 in the case of SFRSCC.

then progressively moved along the centerline towards the other end of the slab, filling the formwork in its path. This concrete casting process is schematically depicted in Fig. 1, marked by the gray region/arrow. A more detailed overview of the casting and curing procedures is given in [32] and a micro-structure analysis in [33]. We proceeded from the assumption that the aforementioned casting process would ensure a symmetric fibre orientation that is qualitatively similar to the one shown in Fig. 1, i.e., the fibres that would eventually be closer to the longer edges of the slab (formwork walls) tend to align more in the direction of the casting point path (centerline), and the fibres that would be closer to the casting point path tend to orient more perpendicularly to it [34,35].

Each created beam is subjected to destructive four-point bending test (described below). The test determines the beam loading history as a function of the beam deflection s registered at the beam midpoint $F(s)$. The main cracking, i.e. the first major crack, is defined by the following condition

$$R(s) = \frac{dF(s)}{ds} = 0, \tag{1}$$

where $F(s)$ is the measured beam loading history and $R(s)$ is the history of flexural rigidity (stiffness). The flexural strength at the moment of cracking is given as

$$\sigma = \frac{F_{\mathrm{f}}L}{bh^2}, \tag{2}$$

where $F_{\mathrm{f}} \equiv F(s_{\mathrm{f}})$ is the fail load and s_{f} is the beam midpoint deflection corresponding to the main cracking; L is the effective length of the beam, see Fig. 3, b and h are the width and height of the beam cross-section mentioned above. Energy absorption history is presented as

$$E(s) = \int F(s)ds. \tag{3}$$

Pre-cracking absorbed energy is defined by

$$E|_{s \in [0, s_{\mathrm{f}})} = \int_0^{s_{\mathrm{f}}} F(s)ds, \tag{4}$$

and post-cracking absorbed energy by

$$E|_{s\in(s_{\mathrm{f}},s_{\mathrm{s}}]} = \int_{s_{\mathrm{f}}}^{s_{\mathrm{s}}} F(s)ds, \tag{5}$$

where $s_{\mathrm{s}} \approx 7$ mm is the maximum deflection achieved/allowed during a bending test. Total absorbed energy is expressed as

$$E|_{s\in[0,s_{\mathrm{s}}]} = \int_{0}^{s_{\mathrm{s}}} F(s)ds. \tag{6}$$

Numeric integration of definite integrals, Eqs (4), (5), and (6), in the case of discretized $F(s)$ values is performed numerically by using the trapezoidal integration rule. Discretized samples F_i of force history $F(s)$ are defined as follows: $F_i = F(s_i)$, $s_i = i\Delta s$, and $\Delta s = s_{\mathrm{s}}/N$, where i is the sample index and N is the total number of measured samples. In the current study $N \gtrsim 700$ for all the SFRSCC beams measured. The accepted mean pre-cracking load $\bar{F}$, for $s \in [0, s_{\mathrm{f}})$ is defined by

$$\bar{F}|_{s\in[0,s_{\mathrm{f}})} = \frac{1}{s_{\mathrm{f}}} \int_{0}^{s_{\mathrm{f}}} F(s)ds. \tag{7}$$

The accepted mean post-cracking load $\bar{F}$ for $s \in (s_{\mathrm{f}}, s_{\mathrm{s}}]$ is expressed as

$$\bar{F}|_{s\in(s_{\mathrm{f}},s_{\mathrm{s}}]} = \frac{1}{s_{\mathrm{s}} - s_{\mathrm{f}}} \int_{s_{\mathrm{f}}}^{s_{\mathrm{s}}} F(s)ds. \tag{8}$$

In the case of discretized load history values F_i, it is possible to use the following formula for the arithmetic average:

$$\bar{F}|_{s\in[s_a,s_b]} = \frac{1}{N_{\mathrm{span}}} \sum_{i=a}^{b} F_i, \tag{9}$$

where N_{span} is the number of samples in the span/range over which the average is calculated, a is the index of the discretized deflection value corresponding to the beginning of the range s_a, so that $s_a = a\Delta s$, and b is the index of the last sample of the range s_b, so that $s_b = b\Delta s$.

2.2. Concrete mixture and steel fibres

The SFRSCC mixture is prepared by using a regular off-the-shelf concrete mixer with a capacity of 2 m^3 and the SCC mix specified in Table 1. SCC is turned into SFRSCC via a gradual addition of a small amount of extra water and hooked-ended steel fibres, shown in Fig. 2 (single fibre). The fibres are added gradually in small batches to prevent possible fibre clustering until fibre content of 0.64% by volume is reached, corresponding to 50 kg/m^3. The geometric, physical and other properties of the fibres are shown in Table 2. The slump flow test of the wet SFRSCC mixture results in the slump diameter of 0.65 m.

The compressive strength after 28 days in the case of SCC was 68.6 MPa (stdev 2 MPa) and in the case of SFRSCC 56.6 MPa (stdev 1 MPa), the individual test results are available in [32].

**Table 1.** Composition of SCC and SFRSCC, the amount mixed 1.0 m^3

Ingredient	Amount (kg)
Cement	330
Sand (0–2 mm)	398
Sand (0–4 mm)	505
Crushed Stone (2–5)	336
Crushed Stone (8–11)	539
Filler	80
Admixture	5.1
Water	175
Fibres (SFSCC only)	50
Extra water (SFSCC only)	≈ 10
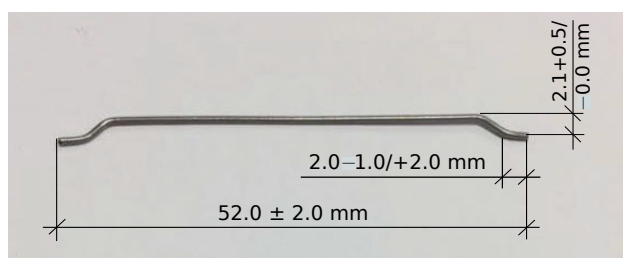
Fig. 2. Steel fibre used in the wet SFRSCC mix.

Table 2. Information on the steel fibres as provided by the manufacturer [36]

Manufacturer	Severstal Metiz
Model	Hendix prime 75/52
Type	Hooked end
Length	52 ± 2 mm
Diameter	0.75 ± 0.04 mm
Bend angle	$(40 \pm 5)°$
Tensile strength	1.5 GPa
Elastic modulus	≥ 190 GPa
Number of fibres	$\approx 5.5 \cdot 10^3$ kg^{-1}

2.3. Destructive four-point bending test

The four-point bending test set-up is shown schematically in Fig. 3. The beams are deformed by means of the universal electro-mechanical/hydraulic testing machine "EU100", manufactured by VEB Werkstoffprüf-maschinen Leipzig. The mechanical load F accepted by a beam is measured by piezoelectric force sensors "HBM U10M" with a measuring range up to 50 kN and a measurement uncertainty of 50 N. The midspan beam deflection s is measured with the help of displacement sensors "HBM WI/10mm-T" that have the measurement uncertainty of 0.2 mm. Additionally, the universal amplifier/analog-to-digital converter "HBM QuantumX MX840A" is used, manufactured by HBM Hottinger Baldwin Messtechnik GmbH that connects to the aforementioned measurement sensors. Digital data capture and the initial on-the-spot data visualization are performed with the software "CatmanEasy DAQ" which was included in the package of the HBM QuantumX.
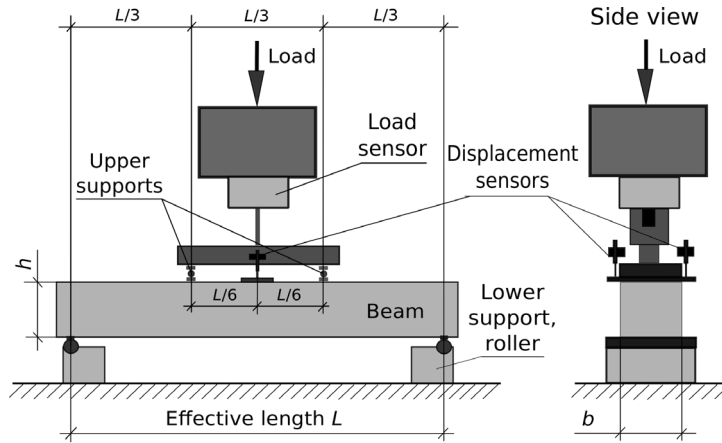
Fig. 3. Schematic drawing of the four-point bending test set-up, where the effective length L is 0.9 m. The zero point for the displacement is on top of a thin plate which is placed across the top of the beam in the centre, at the beginning of the test the displacement gauges are compressed.

3. EXPERIMENTAL RESULTS AND ANALYSIS

3.1. Comparison of SCC beams with SFRSCC beams

Figure 4 illustrates the load history of the selected SCC beams (see Fig. 1). The beams display elastic, mostly constant pre-cracking behaviour with the mean flexural rigidity $\bar{R}|_{s\in[0,\bar{s}_f)} \approx 12.7$ kN/mm, and the post-cracking mean flexural rigidity $\bar{R}|_{s\in(\bar{s}_f,s_s]} \approx -9.5$ kN/mm.

Figure 5 shows: the load history data $F(s)$ for all the 40 beams (see Fig. 1); the average pre-cracking and post-cracking load, and the absorbed energy values; the average load history graph $\bar{F}(s)$; and the absorbed energy history graphs $E(s)$. The following characteristics of the average load history $\bar{F}(s)$ are not indicated in Fig. 5: the mean pre-cracking flexural rigidity $\bar{\bar{R}}|_{s\in[0,\bar{s}_f)} = 12.05 \pm 1.89$ kN/mm, where the uncertainty is understood as a standard deviation of $\bar{R}$ values; the mean post-cracking flexural rigidity $\bar{\bar{R}}|_{s\in(\bar{s}_f,s_s]} = -0.39 \pm 0.20$ kN/mm. These results are calculated slightly differently in comparison to the previous definition of mean values, *cf.* Eqs (7) and (8). The mean (or more precisely the mean of a mean) pre-cracking flexural rigidity $\bar{\bar{R}}$ is expressed as

$$\bar{\bar{R}}|_{s\in[0,\bar{s}_f)} = \frac{1}{40} \sum_{j=1}^{40} \left(\bar{R}|_{s\in[0,s_f)} \right)_j, \tag{10}$$
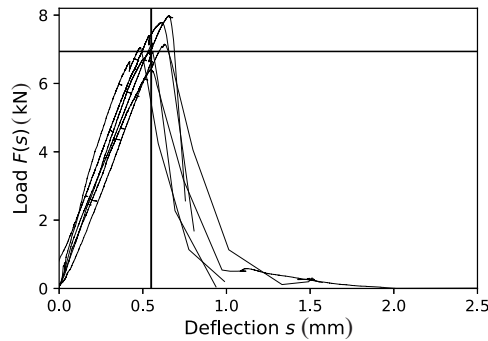
where $j \in [1,40]$ is the beam number and

$$\bar{R}|_{s\in[0,s_f)} = \frac{1}{s_f} \int_0^{s_f} R(s)ds. \tag{11}$$

And, the mean post-cracking flexural rigidity $\bar{\bar{R}}$ is defined by

$$\bar{\bar{R}}|_{s\in(\bar{s}_f,s_s]} = \frac{1}{40} \sum_{j=1}^{40} \left(\bar{R}|_{s\in(s_f,s_s]} \right)_j, \tag{12}$$

where

$$\bar{R}|_{s\in(s_f,s_s]} = \frac{1}{s_s - s_f} \int_{s_f}^{s_s} R(s)ds. \tag{13}$$

Fig. 4. Load history $F(s)$ for the selected SCC beams, shown in Fig. 1. The average deflection corresponding to the main cracking $\bar{s}_{\mathrm{f}} = 0.55$ mm is depicted by the vertical line. The mean cracking load $\bar{F}_{\mathrm{f}} \equiv \bar{F}(\bar{s}_{\mathrm{f}}) \approx 7.0$ kN corresponding to the selected load history graphs is indicated by the horizontal line.
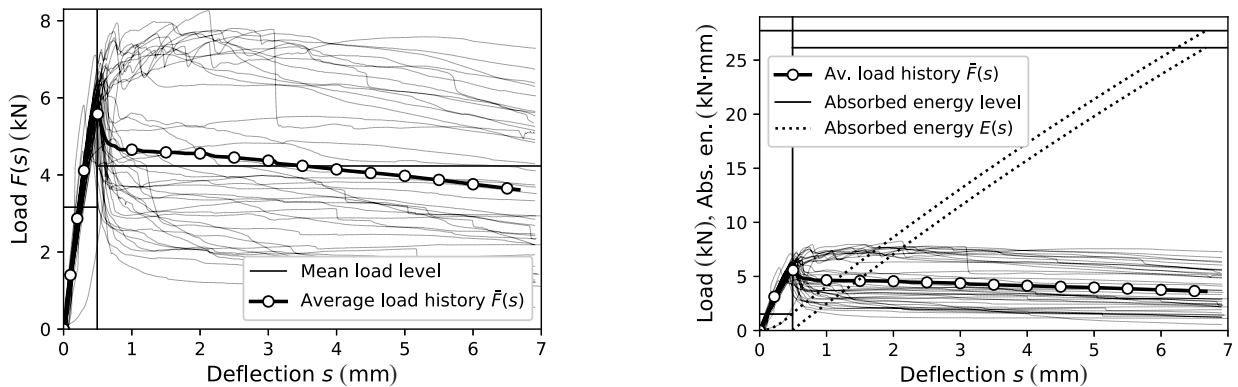
Fig. 5. Load history graphs $F(s)$ for SFRSCC beams No. 1–40 are represented by the thin continuous lines. The load history graph that is shown by the marked thick line is the mean load history $\bar{F}(s)$ averaged over all the 40 measured beam histories. Left: the mean pre-cracking load $\bar{F}|_{s \in [0, \bar{s}_{\mathrm{f}})} = 3.2$ kN, where $\bar{s}_{\mathrm{f}} = 0.50$ mm (indicated by the vertical line), and the mean post-cracking load $\bar{F}|_{s \in (\bar{s}_{\mathrm{f}}, s_{\mathrm{s}}]} = 4.2$ are represented by the horizontal continuous lines. Right: the pre-cracking absorbed energy level $E|_{s \in [0, \bar{s}_{\mathrm{f}})} = 1.5$ kN·mm, the post-cracking absorbed energy level $E|_{s \in (\bar{s}_{\mathrm{f}}, s_{\mathrm{s}}]} = 26.1$ kN·mm, and the total absorbed energy level $E|_{s \in (0, s_{\mathrm{s}}]} = 27.7$ kN·mm are shown by the horizontal continuous lines. The corresponding energy absorption histories $E(s)$ are depicted by the dotted lines.

The comparison of the results shown in Figs 4 and 5 demonstrates clearly that the addition of the fibres changes the post-cracking dynamics of SFRSCC significantly. SFRSCC is capable of accepting significant loading even after cracking of a beam has occurred. The mean pre-cracking flexural rigidity $\bar{R}|_{s \in [0, \bar{s}_{\mathrm{f}})}$ in the case of SCC and $\bar{\bar{R}}|_{s \in [0, \bar{s}_{\mathrm{f}})}$ in the case of SFRSCC are approximately equal, which is expected since as regards small deflections, both materials should behave according to the linear theory. The comparison of the mean cracking loads reveals that in relation to SCC $\bar{F}_{\mathrm{f}} \approx 7.0$ kN and in relation to SFRSCC $\bar{F}_{\mathrm{f}} \approx 5.5$ kN. This counter-intuitive observation can likely be explained by the slightly different water contents in the wet concrete mixtures, see Table 1.

At the first glance the results for SFRSCC beams shown in Fig. 5 seem random. One can observe the beam load histories $F(s)$ with deflection-hardening dynamics and with the opposite, as well. Also, the highly fluctuating mean post-cracking load values can be detected that span from 1.0 to 7.0 kN, approximately. In the following sections the presented data will be analysed and attempted to be organized.

3.2. Effect of dominant fibre orientation on flexural strength

Figure 6 shows the flexural strength σ, Eq. (2), against the beam number. The results are divided into four groups/regions of the original slab: beams 1–10, 11–20, 26–35, and the *centerline* beams. Figure 7 presents
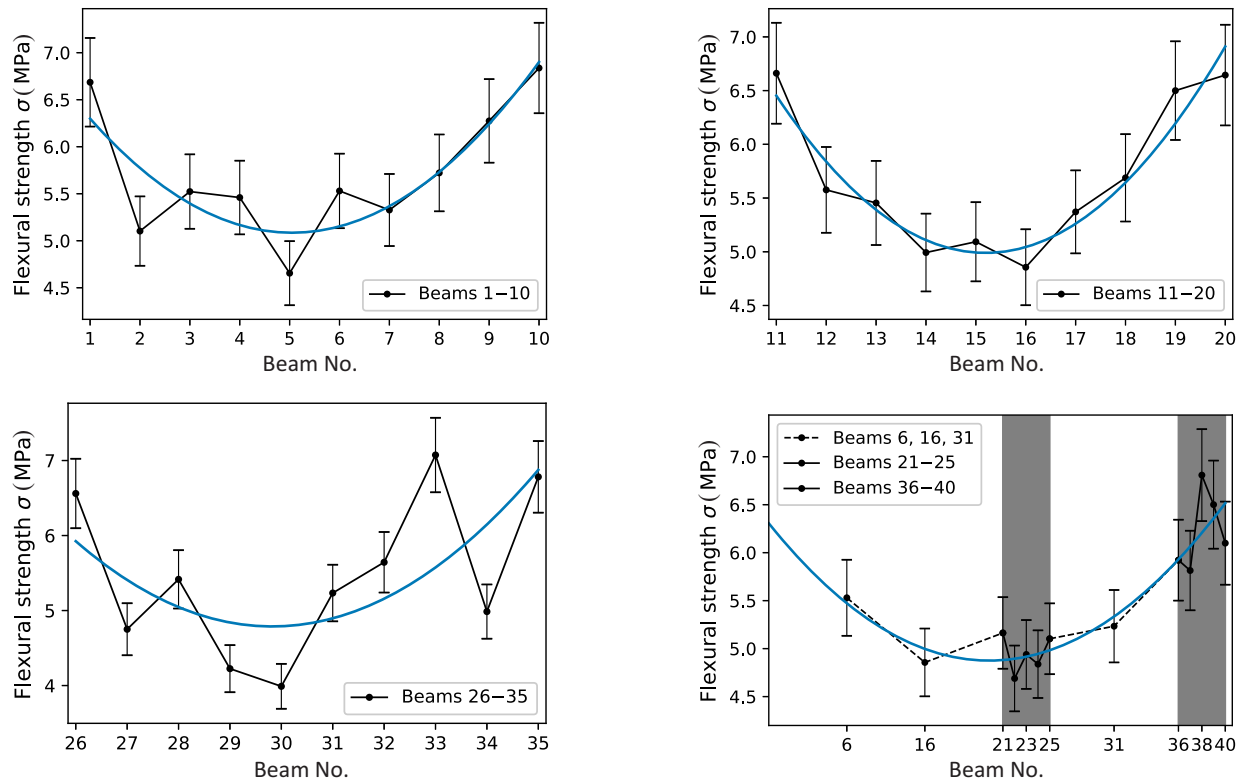
Fig. 6. Flexural strength σ as a function of the beam number. Least square fit graphs of the dominant trends are indicated by using the continuous lines. The lower-right plot corresponds to the centerline results highlighted in Fig. 7.
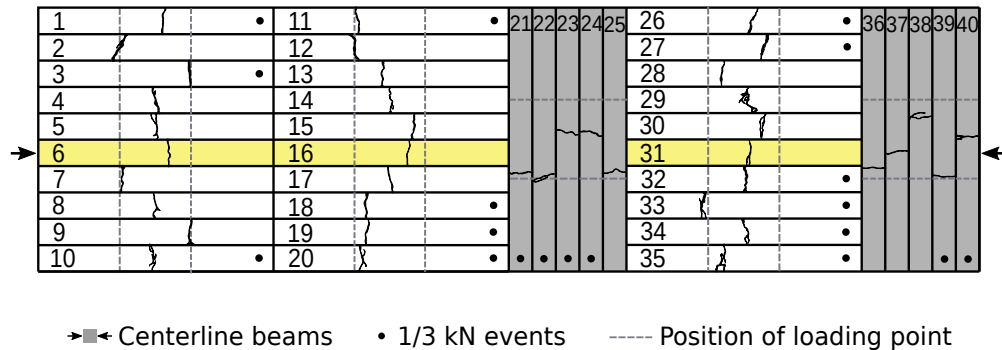

Fig. 7. Centerline beams numbered 6, 16, 21–25, 31, 36–40 are highlighted by the coloured backgrounds and bold arrows. The positions and shapes (bottom view) of the cracks sustained at the main cracking are shown based on the realistic crack patterns.

the numbering and positions of all the 40 beams (the same as in Fig. 1), as well as the four groups of interest, including the centerline beams. The centerline beams represent a cross-section of the original slab in its lengthwise direction. The other groups are cross-sections perpendicular to the longer dimension of the slab.

All the presented results, shown in Fig. 6, feature a parabolic trend. The trend is detected by least square fitting of a second-order polynomial to the shown data points. The beams and thus the slab is stronger near its edges. The relative increase in flexural strength σ near the edges is approximately 20–25% in comparison to the regions closer to the middle. The change in flexural strength σ is relatively gradual and continuous, considering the stochastic and anisotropic nature of the material worked with.

The reason for this strength increase must be related to the fibre orientation [33]. A SFRSCC beam with a favourable dominant fibre orientation is able to better resist the bending. The results presented here serve as a justification/proof to the assumption given in Sec. 2.1 regarding the dominant fibre orientation, see Fig. 1. When even a small fraction of fibres are aligned along the direction of the length of a beam (direction of the tensile stress), they will effectively start to perform similarly to regular steel rebars increasing the effective/average tensile strength of the concrete.

### 3.3. Effect of dominant fibre orientation on mean post-cracking load

Figure 8 demonstrates the accepted mean post-cracking load $\bar{F}|_{s\in(s_\mathrm{f},s_\mathrm{s}]}$ against the beam number. The results presented here are qualitatively identical to the ones shown in Fig. 6. This means that the post-cracking strength and durability characteristic are also governed by the dominant fibre orientation. The beams closer to the edges of the slab accept approximately 50–65% more load compared to the middle region of the slab.

3.4. Effect of dominant fibre orientation on post-cracking absorbed energy

Figure 9 presents the post-cracking absorbed energy $E|_{s\in(s_\mathrm{f},s_\mathrm{s}]}$ against the beam number. Once again the parabolic trends are present. SFRSCC located near the edges of the slab is capable of absorbing approximately 45–65% more energy compared to the concrete located in the middle of the slab. The ability of the material to absorb energy is referred to as its toughness.
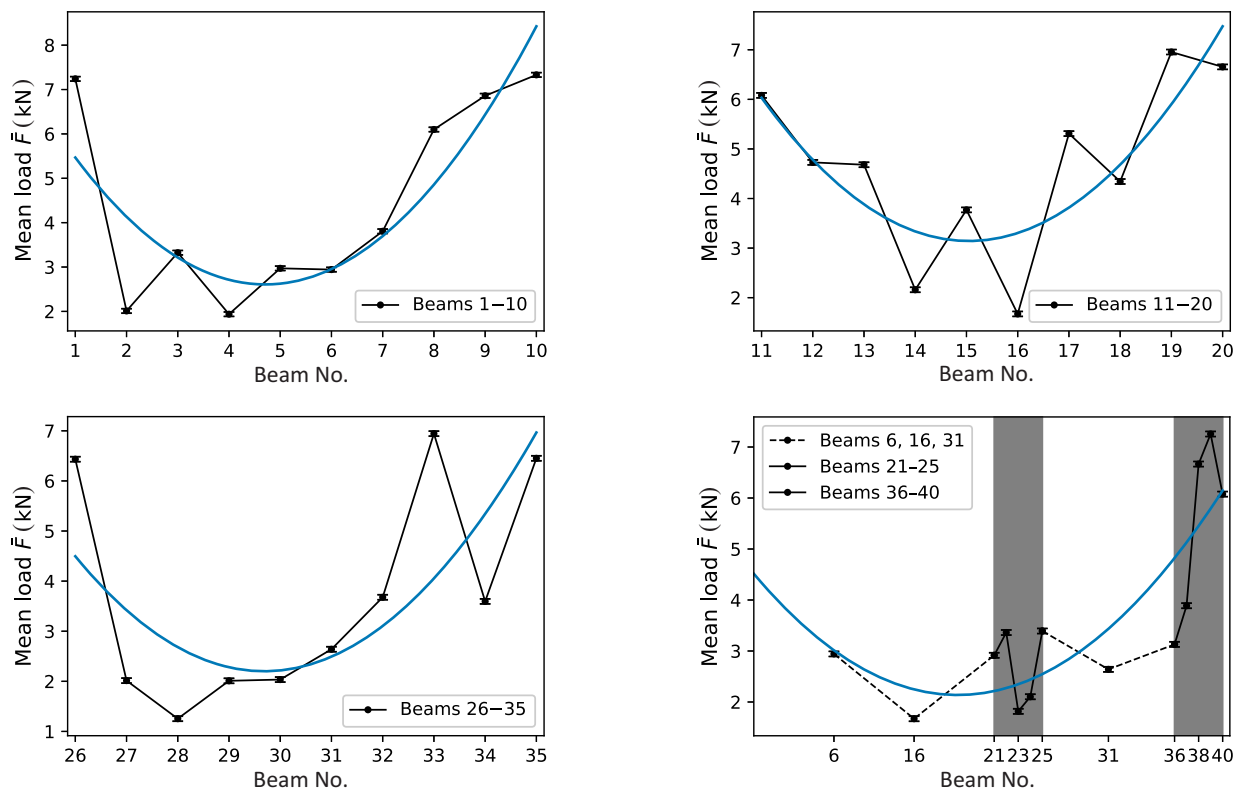
Fig. 8. The accepted mean post-cracking load $\bar{F}|_{s\in(s_\mathrm{f},s_\mathrm{s}]}$ as a function of the beam number. Least square fit graphs of the dominant trends are indicated by the continuous lines. The lower-right plot corresponds to the centerline results highlighted in Fig. 7. The uncertainty of the displayed accepted mean load values $\delta\bar{F}|_{s\in(s_\mathrm{f},s_\mathrm{s}]} = \pm 50$ N.
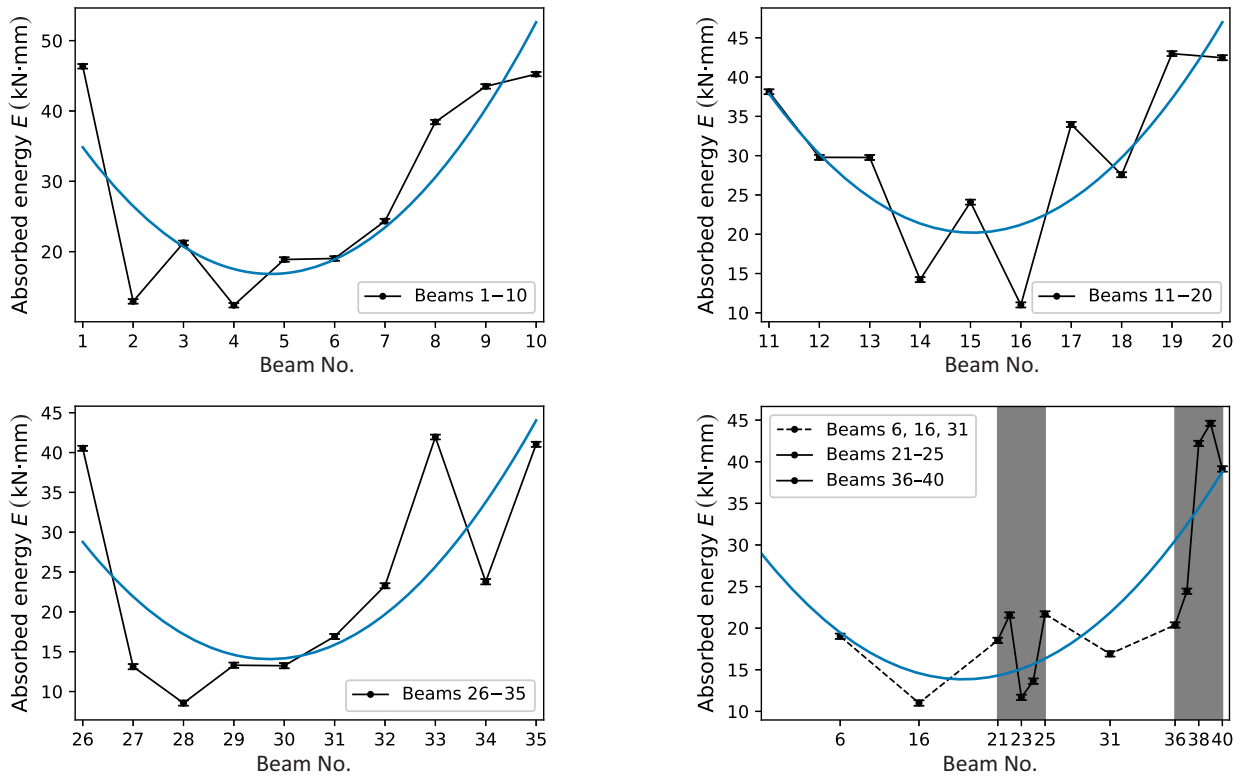
Fig. 9. Post-cracking absorbed energy $E|_{s\in(s_f,s_s]}$ as a function of the beam number. Least square fit graphs of the dominant trends are indicated by the continuous lines. The lower-right plot corresponds to the centerline results highlighted in Fig. 7. The calculated uncertainty of the displayed energy values $\delta E|_{s\in(s_f,s_s]} = \pm\xi$ kN·mm, where $\xi \in [0.30, 0.33]$.

3.5. Dominant fibre orientation and crack position

Figure 7 demonstrates the position and shape of the cracks associated with the main cracking of the beams. The cracks are shown for all the 40 beams. A visual inspection of beams 11–20 seems to suggest that the stronger beams, located closer to the edges of the slab, tend to crack near the upper support points of the four-point bending machine shown in Fig. 3. This may be explained by the interplay of shear stresses and bending moments. The normal force introduced by the support simply cuts through/pushes itself into the material. In the other regions of the slab this phenomenon is less observable, being harder to distinguish from a random chance.

4. DISCUSSION

In addition to the post-cracking results discussed in Secs 3.3 and 3.4, the authors of this paper also considered the mean pre-cracking accepted load $\bar{F}|_{s\in[0,s_f)}$, the total mean load $\bar{F}|_{s\in[0,s_s]}$, the pre-cracking absorbed energy $E|_{s\in[0,s_f)}$, and the total absorbed energy $E|_{s\in[0,s_s]}$ values. It was established that all of these values when plotted against the beam numbers and for the four regions of interest discussed in Sec. 3.2 have graphs qualitatively similar to the ones shown in Figs 8 and 9. The results regarding the mean pre-cracking load $\bar{F}|_{s\in[0,s_f)}$ and the pre-cracking absorbed energy $E|_{s\in[0,s_f)}$ mean that in a linear regime of loading the SFRSCC strength depends also on the dominant fibre orientation. The intact and loaded SFRSCC is stronger when the fibres are oriented in the direction of the tensile stresses.

While analysing the data presented in this paper, an interesting observation was made. The load history $F(s)$ curves of the individual beams feature step-shaped cracking events that are temporally highly located.
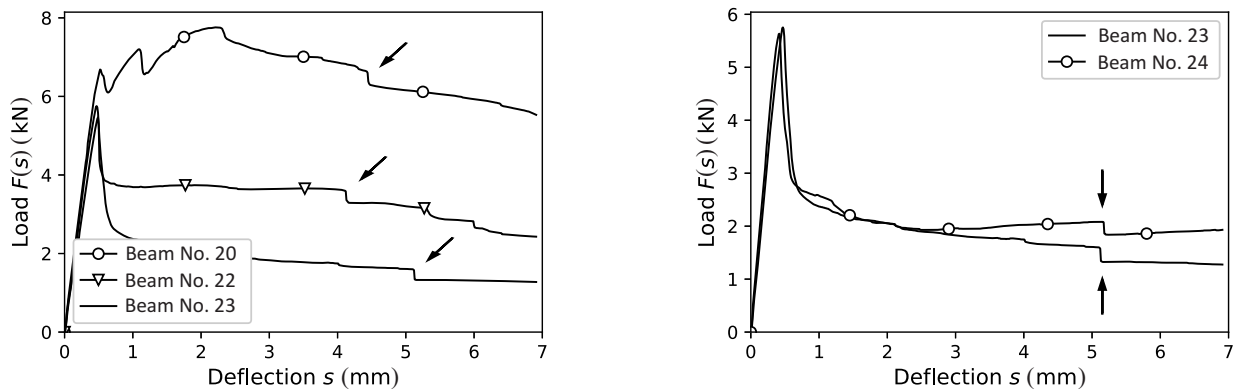
Fig. 10. Left: Examples of 1/3 kN events. The events are indicated by the bold arrows. Right: An example of neighbouring beams where the 1/3 kN events occurred almost precisely at the same beam deflection value *s*.

What is interesting about these events is the fact that the drop in the accepted load F is consistently almost precisely 1/3 kN. The examples regarding the 1/3 kN events are presented in Fig.10. The beams featuring in the events are shown in Fig.7. Almost half (47.5%) of the beams feature in at least one 1/3 kN event. In one instance an event spans two neighbouring beams, beams 23 and 24, see Fig.10. A satisfactory explanation supported by evidence regarding the cause/source of the 1/3 kN events has not been identified by the authors.

5. CONCLUSIONS

This paper presents the results of an experimental investigation into the effects of the fibre orientation on the flexural strength and fracture toughness of SFRSCC. The destructive four-point bending testing was used to measure the flexural strength at the main cracking (Sec. 3.2), the accepted mean post-cracking loading (Sec. 3.3), and energy absorption capacity (toughness) of the concrete (Sec. 3.4)

It was shown that a *favourable* fibre orientation, where the fibres are oriented in the direction of tensile stresses, would increase the flexural strength of the SFRSCC beams with dimensions of 0.1 m × 0.1 m × 1.0 m, up to 25% (approximately 20–25%), the accepted mean post-cracking loading up to 65% (approximately 50–65%), and the absorbed energy levels up to 65% (approximately 45–65%) for the specific concrete mixture used, see Table 1.

The presented results and analysis demonstrate the importance of the dominant fibre orientation on the final strength and toughness characteristics of hardened SFRSCC. If a concrete slab with uniform and isotropic strength characteristics is required, one needs to ensure a random fibre orientation throughout the material. Open pour casting, where the concrete mix is subjected to a free-surface flow, as was described in Sec. 2.1, can – and often will – result in an uneven strength distribution, see Figs 6, 8, and 9. This uneven strength and toughness distribution should be taken into consideration in construction guidelines and specially trained staff may be required for the casting of SFRSCC to ensure the desired properties.

CREDIT AUTHORSHIP CONTRIBUTION STATEMENT

Dmitri Kartofelev: Investigation, Formal analysis, Writing – Original draft. **Oksana Goidyk**: Investigation – Conducting experiments, Formal analysis, Writing – Original draft. **Heiko Herrmann**: Conceptualization, Methodology, Investigation – Planning and conducting experiments, Writing – Review and editing, Project administration, Funding acquisition.

ACKNOWLEDGEMENTS

REFERENCES

1. Brandt, A. M. Fibre reinforced cement-based (FRC) composites after over 40 years of development in building and civil engineering. *Compos. Struct.*, 2008, **86**(1–3), 3–9.
2. Błaszczyński, T. and Przybylska-Fałek, M. Steel fibre reinforced concrete as a structural material. *Procedia Eng.*, 2015, **122**, 282–289.
3. Naaman, A. E. High performance fiber reinforced cement composites: classification and applications. In *CBM-CI international workshop, Karachi, Pakistan*, 2007, 389–401.
4. Di Prisco, M., Plizzari, G., and Vandewalle, L. Fibre reinforced concrete: new design perspectives. *Mater. Struct.*, 2009, **42**(9), 1261–1281.
5. Domone, P. L. Self-compacting concrete: an analysis of 11 years of case studies. *Cem. Concr. Compos.*, 2006, **28**(2), 197–208.
6. Vicente, M. A., Gonzalez, D. C., and Mínguez, J. Determination of dominant fibre orientations in fibre-reinforced high-strength concrete elements based on computed tomography scans. *Nondestr. Test. Eval.*, 2014, **29**(2), 164–182.
7. Laranjeira, F., Aguado, A., Molins, C., Grunewald, S., Walraven, J., and Cavalaro, S. H. P. Framework to predict the orientation of fibers in FRC: a novel philosophy. *Cem. Concr. Res.*, 2012, **42**(6), 752–768.
8. Vandewalle, L., Heirman, G., and Van Rickstal, F. Fibre orientation in self-compacting fibre reinforced concrete. In *Proc. of the 7th Int. RILEM Symp. on Fibre Reinforced Concrete: Design and Applications (BEFIB2008)*. 2008, 719–728.
9. Zerbino, R., Tobes, J. M., Bossio, M. E., and Giaccio, G. On the orientation of fibres in structural members fabricated with self compacting fibre reinforced concrete. *Cem. Concr. Compos.*, 2012, **34**(2), 191–200.
10. Michels, J. and Gams, M. Preliminary study on the influence of fibre orientation in fibre reinforced mortars. *Gradevinar*, 2016, **68**(8), 645–655.
11. Mínguez, J., González, D. C., and Vicente, M. A. Fiber geometrical parameters of fiber-reinforced high strength concrete and their influence on the residual post-peak flexural tensile strength. *Constr. Build. Mater.*, 2018, **168**, 906–922.
12. González, D. C., Minguez, J., Vicente, M. A., Cambronero, F., and Aragón, G. Study of the effect of the fibers' orientation on the post-cracking behavior of steel fiber reinforced concrete from wedge-splitting tests and computed tomography scanning. *Constr. Build. Mater.*, 2018, **192**, 110–122.
13. Eik, M., Puttonen, J., and Herrmann, H. An orthotropic material model for steel fibre reinforced concrete based on the orientation distribution of fibres. *Compos. Struct.*, 2015, **121**, 324–336.
14. Eik, M., Puttonen, J., and Herrmann, H. The effect of approximation accuracy of the orientation distribution function on the elastic properties of short fibre reinforced composites. *Compos. Struct.*, 2016, **148**, 12–18.
15. Herrmann, H. An Improved Constitutive Model for Short Fibre Reinforced Cementitious Composites (SFRC) Based on the Orientation Tensor. In *Generalized Continua as Models for Classical and Advanced Materials* (Altenbach, H. and Forest, S., eds), Springer International Publishing, Cham, 2016, 213–227.
16. Laranjeira, F., Grunewald, S., Walraven, J., Blom, C., Molins, C., and Aguado, A. Characterization of the orientation profile of steel fiber reinforced concrete. *Mater. Struct.*, 2011, **44**(6), 1093–1111.
17. Herrmann, H. and Lees, A. On the influence of the rheological boundary conditions on the fibre orientations in the production of steel fibre reinforced concrete elements. *Proc. Estonian Acad. Sci.*, 2016, **65**(4), 408–413.
18. Martinie, L. and Roussel, N. Simple tools for fiber orientation prediction in industrial practice. *Cem. Concr. Res.*, 2011, **41**(10), 993–1000.
19. Torrijos, M. C., Barragán, B. E., and Zerbino, R. L. Placing conditions, mesostructural characteristics and post-cracking response of fibre reinforced self-compacting concretes. *Constr. Build. Mater.*, 2010, **24**(6), 1078–1085.
20. Dupont, D. and Vandewalle, L. Distribution of steel fibres in rectangular sections. *Cem. Concr. Compos.*, 2005, **27**(3), 391–398.
21. Zhou, B. and Uchida, Y. Influence of flowability, casting time and formwork geometry on fiber orientation and mechanical properties of UHPFRC. *Cem. Concr. Res.*, 2017, **95**, 164–177.
22. Pajak, M. and Ponikiewski, T. Flexural behavior of self-compacting concrete reinforced with different types of steel fibers. *Constr. Build. Mater.*, 2013, **47**, 397–408.
23. Rizzuti, L. and Bencardino, F. Effects of fibre volume fraction on the compressive and flexural experimental behaviour of SFRC. *Contemp. Eng. Sci.*, 2014, **7**(8), 379–390.
24. Liu, R. and Liu, Y. Steel fiber reinforced concrete and its application performance. *Int. J. Multidiscip. Res. Dev.*, 2016, **3**(6), 341–343.

25. Alberti, M. G., Enfedaque, A., and Gálvez, J. On the mechanical properties and fracture behavior of polyolefin fiber reinforced self-compacting concrete. *Constr. Build. Mater.*, 2014, **55**, 274–288.
26. Stahli, P. and Van Mier, J. G. M. Manufacturing, fibre anisotropy and fracture of hybrid fibre concrete. *Eng. Fract. Mech.*, 2007, **74**(1–2), 223–242.
27. Kim, D. J., Park, S. H., Ryu, G. S., and Koh, K. T. Comparative flexural behavior of hybrid ultra high performance fiber reinforced concrete with different macro fibers. *Constr. Build. Mater.*, 2011, **25**(11), 4144–4155.
28. Vicente, M. A., Mínguez, J., and González, D. C. Computed tomography scanning of the internal microstructure, crack mechanisms, and structural behavior of fiber-reinforced concrete under static and cyclic bending tests. *Int. J. Fatigue*, 2019, **121**, 9–19.
29. Kang, S.-T. and Kim, J.-K. Numerical simulation of the variation of fiber orientation distribution during flow molding of ultra high performance cementitious composites (UHPCC). *Cem. Concr. Compos.*, 2012, **34**(2), 208–217.
30. Svec, O., Skocek, J., Stang, H., Olesen, J. F., and Poulsen, P. N. Flow simulation of fiber reinforced self compacting concrete using lattice Boltzmann method. In *Dissemination. 8th International Congress on the Chemistry of Cement, Madrid, Spain, July 3-8*, 2011.
31. The OpenFOAM Foundation Ltd, 2020. OpenFOAM. https://openfoam.org/
32. Herrmann, H., Goidyk, O., Naar, H., Tuisk, T., and Braunbrück, A. The influence of fibre orientation in self-compacting concrete on 4-point bending strength. *Proc. Estonian Acad. Sci.*, 2019, **68**(3).
33. Herrmann, H., Boris, R., Goidyk, O., and Braunbrück, A. Variation of bending strength of fiber reinforced concrete beams due to fiber distribution and orientation and analysis of microstructure. *IOP Conf. Ser.: Mater. Sci. Engineering*, 2019, **660**, 012059.
34. Boulekbache, B., Hamrat, M., Chemrouk, M., and Amziane, S. Flowability of fibre-reinforced concrete and its effect on the mechanical properties of the material. *Constr. Build. Mater.*, 2010, **24**(9), 1664–1671.
35. Herrmann, H., Goidyk, O., and Braunbrück, A. Influence of the flow of self-compacting steel fiber reinforced concrete on the fiber orientations, a report on work in progress. In *Short Fibre Reinforced Cementitious Composites and Ceramics* (Herrmann, H. and Schnell, J., eds). Springer, 2019, 97–110.
36. Severstal Metiz. Hendix prime 75/52 – hooked ends fiber. http://www.severstalmetiz.ru

Teraskiudbetoonplaadi tugevuse mittehomogeensuse sõltuvus teraskiudude ruumilisest orientatsioonist

Dmitri Kartofelev, Oksana Goidyk ja Heiko Herrmann

Käesolevas eksperimentaalses artiklis on uuritud isetihenduva kiudbetooni tugevuse sõltuvust teraskiudude ruumilisest orientatsioonist ja betooni valuprotseduurist. Tugevuskarakteristikute mõõtmiseks kasutati purustavat nelja punkti paindekatset. Mõõtmistulemuste analüüs näitas, et teraskiudude *soositud* orientatsioon tõstab betoontala paindetugevust kuni 25%, keskmist purunemisjärgset vastuvõetud koormust kuni 65% ja plastse energia absorbeerimise võimet kuni 65%. Käesoleva artikli tulemused näitavad teraskiudude jaotustiheduse ja ruumilise orientatsioonilise jaotuse tähtsust lõpp-produkti üldisele tugevusele. Töös esitatud järeldused kehtivad ka teistele kiududega tugevdatud metamaterjalidele.